Acta Pharmaceutica Sinica B 2025;15(1):188−204

Chinese Pharmaceutical Association
Institute of Materia Medica, Chinese Academy of Medical Sciences

Acta Pharmaceutica Sinica B

www.elsevier.com/locate/apsb
www.sciencedirect.com

ORIGINAL ARTICLE

Tumor-intrinsic PRMT5 upregulates FGL1 *via* methylating TCF12 to inhibit CD8$^+$ T-cell-mediated antitumor immunity in liver cancer

Jiao Sun[a,b,†], Hongfeng Yuan[a,†], Linlin Sun[a,b,†], Lina Zhao[a], Yufei Wang[a], Chunyu Hou[a], Huihui Zhang[a], Pan Lv[a], Guang Yang[a,*], Ningning Zhang[b,*], Wei Lu[b,*], Xiaodong Zhang[a,*]

[a]*State Key Laboratory of Drug ability Evaluation and Systematic Translational Medicine, Tianjin's Clinical Research Center for Cancer, Tianjin Key Laboratory of Digestive Cancer/Department of Gastrointestinal Cancer Biology, Tianjin Cancer Institute, Liver Cancer Center, National Clinical Research Center for Cancer, Tianjin Medical University Cancer Institute and Hospital, Tianjin 300060, China*
[b]*Department of Hepatobiliary Oncology, Liver Cancer Center, Tianjin Medical University Cancer Institute and Hospital, Key Laboratory of Cancer Prevention and Therapy, Tianjin's Clinical Research Center for Cancer, National Clinical Research Center for Cancer, Tianjin 300060, China*

Received 17 June 2024; received in revised form 22 August 2024; accepted 12 October 2024

KEY WORDS

PRMT5;
TCF12;
FGL1;
Antitumor immunity;
Liver cancer

Abstract Protein arginine methyltransferase 5 (PRMT5) acts as an oncogene in liver cancer, yet its roles and in-depth molecular mechanisms within the liver cancer immune microenvironment remain mostly undefined. Here, we demonstrated that disruption of tumor-intrinsic PRMT5 enhances CD8$^+$ T-cell-mediated antitumor immunity both *in vivo* and *in vitro*. Further experiments verified that this effect is achieved through downregulation of the inhibitory immune checkpoint molecule, fibrinogen-like protein 1 (FGL1). Mechanistically, PRMT5 catalyzed symmetric dimethylation of transcription factor 12 (TCF12) at arginine 554 (R554), prompting the binding of TCF12 to FGL1 promoter region, which transcriptionally activated FGL1 in tumor cells. Methylation deficiency at TCF12-R554 residue downregulated FGL1 expression, which promoted CD8$^+$ T-cell-mediated antitumor immunity. Notably, combining the PRMT5 methyltransferase inhibitor GSK591 with PD-L1 blockade efficiently inhibited

*Corresponding authors.
E-mail addresses: zhangxiaodong@tjmuch.com (Xiaodong Zhang), luwei__1966@163.com (Wei Lu), mail3ningning@163.com (Ningning Zhang), yangguang@tjmuch.com (Guang Yang).
[†]These authors made equal contributions to this work.
Peer review under the responsibility of Chinese Pharmaceutical Association and Institute of Materia Medica, Chinese Academy of Medical Sciences.

https://doi.org/10.1016/j.apsb.2024.10.016

liver cancer growth and improved overall survival in mice. Collectively, our findings reveal the immunosuppressive role and mechanism of PRMT5 in liver cancer and highlight that targeting PRMT5 could boost checkpoint immunotherapy efficacy.

1. Introduction

Liver cancer is known for its high incidence and mortality rates, with more than 900,000 new cases and over 830,000 deaths worldwide annually[1]. Notably, most patients are not eligible for surgery at the time of diagnosis and exhibit insensitivity to conventional treatments such as radiotherapy and chemotherapy[2,3]. Hence, it is imperative to explore more effective treatment strategies. Numerous studies have highlighted the crucial role of the tumor immune microenvironment (TIME) in the progression of liver cancer[4]. Limited knowledge of TIME hinders the development of effective treatments. Therefore, gaining deeper insights into immune microenvironment of liver cancer and developing modulatory strategies may offer new therapeutic strategies.

Protein arginine methyltransferase 5 (PRMT5), a member of the protein arginine methyltransferases (PRMTs) family, plays a significant role in transcriptional and post-transcriptional regulation of target molecules by arginine methylation of histone or non-histone substrates[5,6]. Accumulating evidence has shown that PRMT5 exerts critical regulatory roles in antitumor immunity[7,8]. Extensive studies have established that PRMT5 significantly enhances cell proliferation, invasion, and metastasis in liver cancer[9,10]. Yet, its immunologic regulatory function in liver cancer remains unclear. Given the potential of PRMT5 in immune regulation and its notable impact on liver cancer, it is necessary to further investigate its role in liver cancer immunity and assess its potential as a therapeutic target.

Tumor infiltrating lymphocytes (TILs), key mediators of antitumor immunity within the tumor microenvironment, are tightly regulated by various co-inhibitory immune checkpoints[11]. Malignant tumors often manipulate the aberrant expression of these checkpoint molecules for immune evasion. Currently, therapies blocking immune checkpoint receptors or ligands, including PD-1 and PD-L1, have become an important approach for enhancing antitumor immunity[12]. Therapies targeting PD-1/PD-L1 have also been employed in liver cancer treatment, yet the objective response rate (ORR) is merely 14%−20%[13]. This limited efficacy may be attributed to the presence of other co-inhibitory immune checkpoints[14]. Consequently, the focus of current research has shifted toward investigating novel immune checkpoints to enhance the efficacy of immunotherapy[15]. Lymphocyte-activation gene 3 (LAG3), a notable immune checkpoint predominantly expressed on the surface of lymphocytes including $CD4^+$ and $CD8^+$ T cells. LAG3 delivers inhibitory signals that are key in regulating immune cell homeostasis, the activation and proliferation of T cells, cytokine production, and cytolytic activity[16-18]. Recent studies have demonstrated that fibrinogen-like protein 1 (FGL1) acts as a primary immune inhibitory ligand for LAG3, and elevated FGL1 levels are correlated with reduced responsiveness to anti-PD-1 therapy[19]. Elevated FGL1 expression in liver cancer tissues and circulating tumor cells is associated with a worse prognosis for patients[20,21]. Concurrently, targeting FGL1 has been shown to enhance immunotherapy efficacy in liver cancer[22]. Thus, modulating FGL1 could be a crucial approach to counteract the poor response to immunotherapy in liver cancer. However, the regulatory mechanism of FGL1 in liver cancer remains unclear.

In this study, we investigated the role of PRMT5 in the immune regulatory function within liver cancer. Strikingly, we found that PRMT5 in liver cancer cells suppresses $CD8^+$ T-cell function by upregulating FGL1, thereby facilitating immune evasion. Notably, PRMT5 inhibitors enhanced the effectiveness of PD-L1 mAb against liver cancer by promoting $CD8^+$ T-cell activation and infiltration within the tumor microenvironment. Our research elucidates the role and mechanism by which PRMT5 drives immunosuppression in liver cancer, and underscores the potential of PRMT5 inhibitors as novel adjuvants to potentiate the efficacy of immune checkpoint inhibitors (ICIs) in liver cancer immunotherapy.

2. Materials and methods

2.1. Human samples

A total of 55 liver cancer tissue samples along with their respective adjacent tissues were collected from the Tianjin Medical University Cancer Institute and Hospital following a surgical removal procedure. Consents were acquired from every patient. Approval for the study protocol was granted by the Research Ethics Committee at Tianjin Medical University Cancer Institute and Hospital (EK2023028). Patient medical records are detailed in Supporting Information Table S1.

2.2. Cell lines, cell culture

The human liver cancer cell lines HepG2 and Huh7, the mouse liver cancer cell lines Hepa1-6 and H22, as well as the Human Embryonic Kidney 293T (HEK293T) cell line, were acquired from ATCC (American Type Culture Collection) and BFB (Biological Resource Center). Hepa1-6-OVA cells were acquired from Meisen CTCC (Zhejiang, China). *TCF12*-knockout (KO) HepG2, Huh7 and Hepa1-6 cells, crafted using CRISPR/Cas9 genetic editing, were developed by Gene Carer Biotech (Xi'an, China). Oligonucleotide sequences for single guide RNA (sgRNA) can be found in Supporting Information Table S2. Using the methods previously described[23], we successfully established stable knockdown (KD) of PRMT5 in both Hepa1-6 and H22 cell lines, and FGL1 KD was achieved in the H22 cell line, utilizing lentivirus-mediated delivery of short hairpin RNA (shRNA). Table S2 presents the target sequences of the short hairpin's complementary DNA (cDNA). Additionally, PRMT5-KD H22 cells were further engineered to overexpress FGL1 through lentiviral to establish the PRMT5-KD combined with FGL1-overexpression (OE) H22 cell line (PRMT5 KD + FGL1 OE).

Stable cell lines expressing TCF12 (WT) or TCF12 (R554K) were established in TCF12-KO Hepa1-6 cells through lentiviral transfection. Each cell line was grown in DMEM (Gibco, Grand Island, NY, USA), supplemented with 10% fetal bovine serum (FBS, Gibco) and 1% penicillin/streptomycin. PCR confirmed that all these cell lines were free from mycoplasma.

2.3. Plasmids or small interfering RNA (siRNA) generation and transfection

Sangon Biotech (Shanghai, China) produced all the siRNAs. The siRNA sequences are detailed in Table S2. Genscript Biotechnology (Genscript, PisV cataway, NJ, USA) was responsible for constructing all the plasmids employed in our research. The plasmids are enumerated in Supporting Information Table S3. Transfections were conducted utilizing Lipofectamine 3000 (Invitrogen, Carlsbad, CA, USA), adhering to the manufacturer's instructions.

2.4. Immunofluorescence assays

Cells cultured in 12-well plates were first washed using PBS, subsequently fixed using paraformaldehyde, and permeabilized with Triton X-100. Post-permeabilization, they underwent BSA incubation, followed by an overnight treatment with primary antibodies. The binding of these primary antibodies was then detected using secondary antibodies. For visualization, either a confocal or fluorescence microscope was employed. Detailed information about the antibodies utilized can be found in Supporting Information Table S4.

2.5. Immunohistochemistry (IHC) staining

Sections of tumors from liver cancer patients and mice underwent dewaxing. Subsequently, IHC staining was carried out, drawing from previously established methods[24]. The specific antibodies utilized are detailed in Table S4.

2.6. Animal experiments

Female BALB/c nude mice, BALB/c mice, and C57BL/6 mice, aged 5 to 6 weeks, were used to establish subcutaneous liver cancer models. These mice were sourced from VITAL River (Beijing, China). The OT-1 mice were sourced from Cyagen Biosciences (Guangzhou, China).

1) C57BL/6 mice or BALB/c nude mice were subcutaneously inoculated with Hepa1-6 cells (either shPRMT5 or control) at a concentration of 1×10^6 cells per mouse ($n = 5$). Post 27 days of inoculation, the mice were euthanized and tumor samples were extracted for examination.
2) To deplete $CD4^+$ T, $CD8^+$ T, or both $CD4^+$ and $CD8^+$ T cells in C57BL/6 mice, neutralizing antibodies (anti-CD4, anti-CD8, both anti-CD4 and anti-CD8, or control IgG) were obtained from BioLegend (San Diego, CA, USA). The information about the antibodies are detailed in Table S4. These antibodies were administered intraperitoneally at a dose of 200 μg, both four days prior to and one day before the subcutaneous injection of 1×10^6 Hepa1-6 cells. Following inoculation, antibody injections were administered every 3 days at the same dose until the experiments were completed. The mice were divided into 8 groups based on the Hepa1-6 cell inoculation and antibody treatment: IgG, PRMT5 KD + IgG, anti-CD4, PRMT5 KD + anti-CD4, anti-CD8, PRMT5 KD + anti-CD8, anti-CD4 + anti-CD8, and PRMT5 KD + anti-CD4 + anti-CD8 ($n = 6$). Post 27 days of inoculation, the mice were euthanized, and tumors were harvested for subsequent examinations and analyses. Additionally, mice subjected to the same treatment were observed for their survival time ($n = 8$). The observation endpoint was defined as when the mouse's tumor volume exceeded 1.5 cm^3, death occurred, or survival reached the 60th day.
3) Ctrl, PRMT5-KD, FGL1-KD and PRMT5-KD + FGL1-OE H22 cell lines were used for subcutaneous tumor inoculation in BALB/c mice. Ctrl, TCF12 KO, TCF12 KO + TCF12 (WT), and TCF12 KO + TCF12 (R554K) Hepa1-6 cell lines were used for subcutaneous tumor inoculation in C57BL/6 mice. Post 27 days of inoculation, the mice were euthanized and tumor samples were extracted for examination.
4) C57BL/6 mice were subcutaneously inoculated with Hepa1-6 cells at a concentration of 1×10^6 cells per mouse. After 11 days post-inoculation, the mice were distributed into four distinct groups: the control group treated with DMSO and IgG2b isotype control (BioXcel, Lebanon, NH, USA) (administered intraperitoneally), the GSK591 (AbMole BioScience, Houston, TX, USA) groups receiving 80 mg/kg doses intraperitoneally every other day, the PD-L1 mAb (BioXcel, Lebanon, NH, USA) group getting 100 μg per mouse intraperitoneally on Days 11, 15, 19, and 23, and lastly, the combined GSK591 with PD-L1 mAb group ($n = 6$). At the end of 32 days from the initial injection, the mice were euthanized, and tumors were extracted for further analysis. Additionally, mice subjected to the same treatment were observed for their survival time ($n = 8$). The observation endpoint was defined as when the mouse's tumor volume exceeded 1.5 cm^3, death occurred, or survival reached the 60th day.

Tumor volume was determined employing Eq. (1):

$$\text{Tumor volume} = 0.52 \times (L \times W \times H) \quad (1)$$

where '*L*' denotes length, '*W*' denotes width, and '*H*' denotes height.

$$\text{The tumor growth inhibition value (TGI, \%)} = (1 - \text{Treatment group tumor mean weight/Control group tumor mean weight}) \times 100 \quad (2)$$

All animal experiments were conducted in accordance with the Declaration of Helsinki and approved by the Tianjin Medical University Cancer Institute and Hospital Animal Care and Use Committee.

2.7. Reverse transcription quantitative PCR (qPCR)

Using Trizol reagent (Solarbio, Beijing, China), total RNA was isolated from the cells or tissues. The obtained RNA was then reverse transcribed with the assistance of cDNA Synthesis SuperMix (Yeasen, Shanghai, China). The process of quantitative PCR was undertaken using SYBR Green (Yeasen). The $2^{-\Delta\Delta Ct}$ approach was employed to determine variances in gene expression levels. For the purpose of normalization, GAPDH served as

the standard reference. Supporting Information Table S5 offers detailed sequences of the primers that were employed.

2.8. Chromatin immunoprecipitation (ChIP) and Re-ChIP

ChIP assays followed the guidelines provided by Cell Signaling Technology (Danvers, MA, USA). In the ChIP process, the cells were fixed with formaldehyde, which cross-linked and thus preserved protein/DNA interactions. After sonication of the cells, DNA/protein complexes were immunoprecipitated using a specific antibody targeting the DNA-binding protein. Post-immunoprecipitation, the DNA underwent washing and cross-link reversal, followed by proteinase K treatment to remove proteins. The DNA was then purified using columns, and the extracted DNA fragments were quantified using qPCR.

Re-ChIP assays were conducted utilizing the Re-ChIP-IP kit (Active Motif, Shanghai, China). Briefly, complexes obtained from the initial immunoprecipitation were eluted using a specialized buffer. Then, a secondary ChIP reaction was performed with a distinct antibody, different from the first. Following this, cross-links were reversed, and the liberated DNA was subjected to PCR analysis to assess the co-localization of the two proteins at a particular region of interest. Primer specifics can be found in Table S5.

2.9. Luciferase reporter gene assays

Luciferase reporter gene evaluations were conducted as per the guidance provided by the manufacturer. The experimental process was conducted as follows: Liver cancer cells were seeded in 24-well plates and subsequently transfected with 1 μg of either full-length or segmented FGL1 promoter luciferase reporter constructs. The full-length construct, pGL3-2101, spanned from 2000 bp upstream to 100 bp downstream of the transcription start site. Additional segmented constructs included pGL3-1561 (−1460 to +100 bp), pGL3-1021 (−920 to +100 bp), pGL3-661 (−560 to +100 bp), and pGL3-391 (−290 to +100 bp). These constructs were transfected into the specified cells. Additionally, 0.05 μg pRL-TK was utilized for normalization purposes. Two days post the transfection, cells were gathered using a lysis buffer. The measurement of the luciferase activity was executed with the Dual-Luciferase Reporter Assay System (Promega, Madison, WI, USA) in line with the manufacturer's stipulated protocols.

2.10. Co-immunoprecipitation (CoIP) assays

Cells underwent lysis using the Native lysis buffer from Solarbio Science & Technology Co., Ltd. (Beijing, China). Post lysis, they were subjected to an overnight incubation either with control IgG or a designated primary antibody, all at 4 °C. Subsequently, Protein A/G beads, sourced from Thermo Fisher Scientific USA, were introduced to the lysates for 2 h. Following this, the beads underwent five wash cycles with the lysis buffer. Finally, proteins separated from the A/G beads were examined using Western blot analysis. The antibodies used are listed in Table S4.

2.11. GST pull-down assay

Prepare GST-only or GST-TCF12 proteins (purified through *Escherichia coli* (*E. coli*)) and His-PRMT5 protein (purified through HEK293T cells). GST or GST-TCF12 proteins were immobilized on Glutathione-Sepharose beads (Yeasen, Shanghai, China) and mixed with recombinant His-PRMT5 protein, followed by incubation of the mixture at 4 °C for 2 h. Subsequently, the samples were analyzed by immunoblotting.

2.12. In vitro methylation assay

Prepare recombinant GST fusion proteins TCF12 WT and TCF12 R554K (purified through *E. coli* and His-PRMT5 protein (purified through HEK293T cells). In a reaction buffer containing 100 μmol/L *S*-adenosyl-L-methionine iodide (SAM), GST-TCF12 WT/TCF12 R554K proteins and His-PRMT5 protein were incubated at 37 °C for 1 h. After stopping the reaction, the SDS sample buffer was added, and the samples were analyzed by immunoblotting following SDS-PAGE.

2.13. Western blot analysis

Cells or tissues were subjected to protein extraction utilizing a solution composed of RIPA lysis buffer combined with protease inhibitors (Solarbio, Beijing, China). The separated proteins went through SDS-PAGE and were subsequently transferred to nitrocellulose filter membranes. These membranes were then blocked using 5% skimmed milk, followed by incubation with specific antibodies. Visualization was achieved with the aid of an ECL Western Blotting Detection Kit provided by GE Healthcare (Waukesha, WI, USA). Detailed information on the antibodies utilized is available in Table S4.

2.14. Cell proliferation assays

The cell viability (2000 cells per well) of each treatment group was measured using CCK-8 (Solarbio, Beijing, China) following the manufacturer's instructions.

2.15. RNA sequencing (RNA-seq) analysis

HepG2 cells underwent transfection with either control siRNA or PRMT5-specific siRNA. For each variant, three biological replicates were conducted. Post-transfection, the cells were harvested using TRIzol, and RNA-seq analysis was carried out by Majorbio Bio-pharm Technology Co., Ltd. (Shanghai, China). Subsequent data analysis took place on the Majorbio Cloud Platform, accessible at www.majorbio.com. Genes displaying a $|\text{fold change}| \geq 2$ and an adjusted P-value <0.05 were deemed significantly differentially expressed.

2.16. Bioinformatics analysis

The databases hTFtarget, JASPAR and Toolkit were used to predict FGL1 transcription factors. The JASPAR database provided insights into the TCF12 binding sites located within the promoter region of FGL1. The docking analysis of PRMT5 with TCF12 was examined using Discovery Studio software according to the previous methods[25,26]. The structural data for PRMT5 and TCF12 were retrieved from the RCSB Protein Data Bank. The CDOCKER was then utilized to conduct an analysis of the PRMT5 and TCF12 docking.

2.17. Single-cell generation from tumor tissue

The fat, fibrous and necrotic areas were removed from the tumor tissues. The tumor samples were cut into small pieces of 2−4 mm. These segments were then enzymatically dissociated using a

Tumor Dissociation Kit (Miltenyi Biotec, Bergisch Gladbach, Germany). The tumor tissue (0.04−1 g) was dissociated into single-cell suspensions by incubation with an enzymatic cocktail containing 2.35 mL of RPMI 1640, 100 μL of enzyme D, 10 μL of enzyme R, and 12.5 μL of enzyme A. The tissues were incubated at 37 °C with constant rotation for 40 min. Following dissociation, the sample was filtered to eliminate any remaining larger particles from the single-cell suspension.

2.18. *T-cell-mediated tumor cell killing assays*

Mouse $CD8^+$ T cells were isolated from the spleens of C57BL/6 or OT-1 mice using the Mouse $CD8^+$ T Cell Isolation Kit (Miltenyi Biotec). Human peripheral blood mononuclear cells (PBMCs) were purchased from Hycells Biotech (Shanghai, China). Human $CD8^+$ T-cell Isolation Kit (Miltenyi Biotec) was used to enrich $CD8^+$ T cells from PBMCs according to the manufacturer's instructions.

For antigen-specific killing, OT-1 T cells were activated with the SIINFEKL peptide (Sigma). The OT-1 $CD8^+$ T cells were co-cultured with Hepa1-6-OVA cells in direct physical contact for 24 h. For non-antigen-specific killing, $CD8^+$ T cells were preactivated with anti-CD3 and anti-CD28 antibodies, following co-cultured with different target tumor cells not expressing OVA for 72 h.

After co-culture, the plates were washed with PBS to remove $CD8^+$ T cells. The remaining tumor cells were then fixed, stained with crystal violet solution, and quantified by spectrometry at an optical density (OD) of 570 nm.

2.19. *Co-culture experiment*

Tumor cells were seeded into the plates and pre-incubated for 12 h to allow proper attachment. After cell adhesion, $CD8^+$ T cells were added and co-cultured with the target tumor cells for either 48 or 72 h. Samples were analyzed by flow cytometry or ELISA.

2.20. *T-cell migration assays*

Liver cancer cells subjected to various treatments were seeded into the lower chamber of a Transwell system, while pre-activated $CD8^+$ T cells were placed in the upper chamber (membrane pore size: 5 μm). The system was incubated for 24 h to allow for T cell migration. Subsequently, T cells in the lower chamber were collected, fixed with 4% paraformaldehyde, and resuspended in 200 μL of PBS. The number of $CD8^+$ T cells that migrated through the membrane was quantified by analyzing the samples with a flow cytometer for 30 s.

2.21. *T-cell proliferation assay*

Collect $CD8^+$ T cells from the co-culture system described previously. The proliferative ability of these $CD8^+$ T cells was evaluated by measuring Ki67 expression using flow cytometry.

2.22. *Flow cytometry*

Cells were subjected to surface staining using appropriate antibodies. The cells were then fixed and permeabilized using the Cyto-Fast Fix/Perm Buffer Set (BioLegend), followed by staining with antibodies targeting intracellular cytokines such as granzyme B and perforin. Additionally, for the detection of FOXP3 and Ki67, the cells were treated with FOXP3 Permeabilization Buffer (BioLegend). Flow cytometric analysis was carried out using LSRFortessa SORP (BD Biosciences, Franklin Lakes, NJ, USA) and Kaluza software. Antibody information is provided in Table S4.

2.23. *Enzyme-linked immunosorbent assay (ELISA)*

Concentrations of FGL1 and interleukin 2 (IL-2) in the cell culture supernatants sourced from various experimental batches were quantified utilizing an ELISA kit. This process was executed in line with the guidelines provided by the manufacturer (Solarbio, Beijing, China).

2.24. *Statistical analysis*

All data are presented as mean ± standard deviation (SD). All analyses were conducted using GraphPad Prism 8 (Graphpad Software Inc., San Diego, CA, USA). Pearson's correlation coefficient was employed to assess relationships between two variables. Differences between two groups were evaluated using the Student's *t*-test, and for comparisons among three or more groups, one-way ANOVA was utilized. Significance levels are marked as: $^*P < 0.05$, $^{**}P < 0.01$, and $^{***}P < 0.001$. ns, not significant.

3. Results

3.1. *PRMT5 disruption promotes $CD8^+$ T-cell-mediated antitumor immunity suppressing liver cancer growth*

To explore the role of PRMT5 in liver cancer progression, we systematically assessed its expression levels using The Cancer Genome Atlas (TCGA) database and clinical liver cancer tissue samples. Analysis of the TCGA database shows that PRMT5 levels in liver cancer tissues are higher compared to adjacent non-tumor tissues (Supporting Information Fig. S1A). Additionally, assays of clinical samples for PRMT5's mRNA and protein levels demonstrated consistent findings (Fig. S1B−S1D). Moreover, TCGA database revealed that higher PRMT5 expression correlates with decreased overall survival in liver cancer patients (Fig. S1E), indicating an adverse prognostic impact.

PRMT5 was silenced using siRNAs, with siPRMT5#1 achieving optimal knockdown efficiency and selected for subsequent studies (Fig. S1F). RNA-seq analysis was conducted on siPRMT5-treated HepG2 cells to elucidate PRMT5's role in liver cancer. Gene Ontology (GO) analysis showed that the differentially expressed genes (DEGs) predominantly enriched pathways associated with transcriptional regulatory activity and immune system processes (Fig. 1A). Subsequently, to delve into the interplay between PRMT5 and tumor immunology, stable PRMT5-KD Hepa1-6 cells were generated (Fig. S1G) and subcutaneously inoculated into immunocompetent C57BL/6 and immunodeficient BALB/c nude mice (Fig. 1B). Our data reveal that PRMT5 KD inhibited tumor growth in both animal models, with more potent suppression in immunocompetent mice (TGI: 28% and 55%, respectively; Fig. 1C), implying that the immune microenvironment may be involved in PRMT5-mediated tumor growth. Compared to C57BL/6 mice, nude mice possess normally functioning B cells and natural killer (NK) cells yet they exhibit a deficiency in T cells. Thus, we speculated that PRMT5 might modulate T-cell-mediated antitumor immunity. In C57BL/6 mice, immunofluorescence (Fig. 1D) and flow cytometry (Fig. 1E) analyses revealed no significant difference in the infiltration of myeloid-derived suppressor cells (MDSCs), conventional

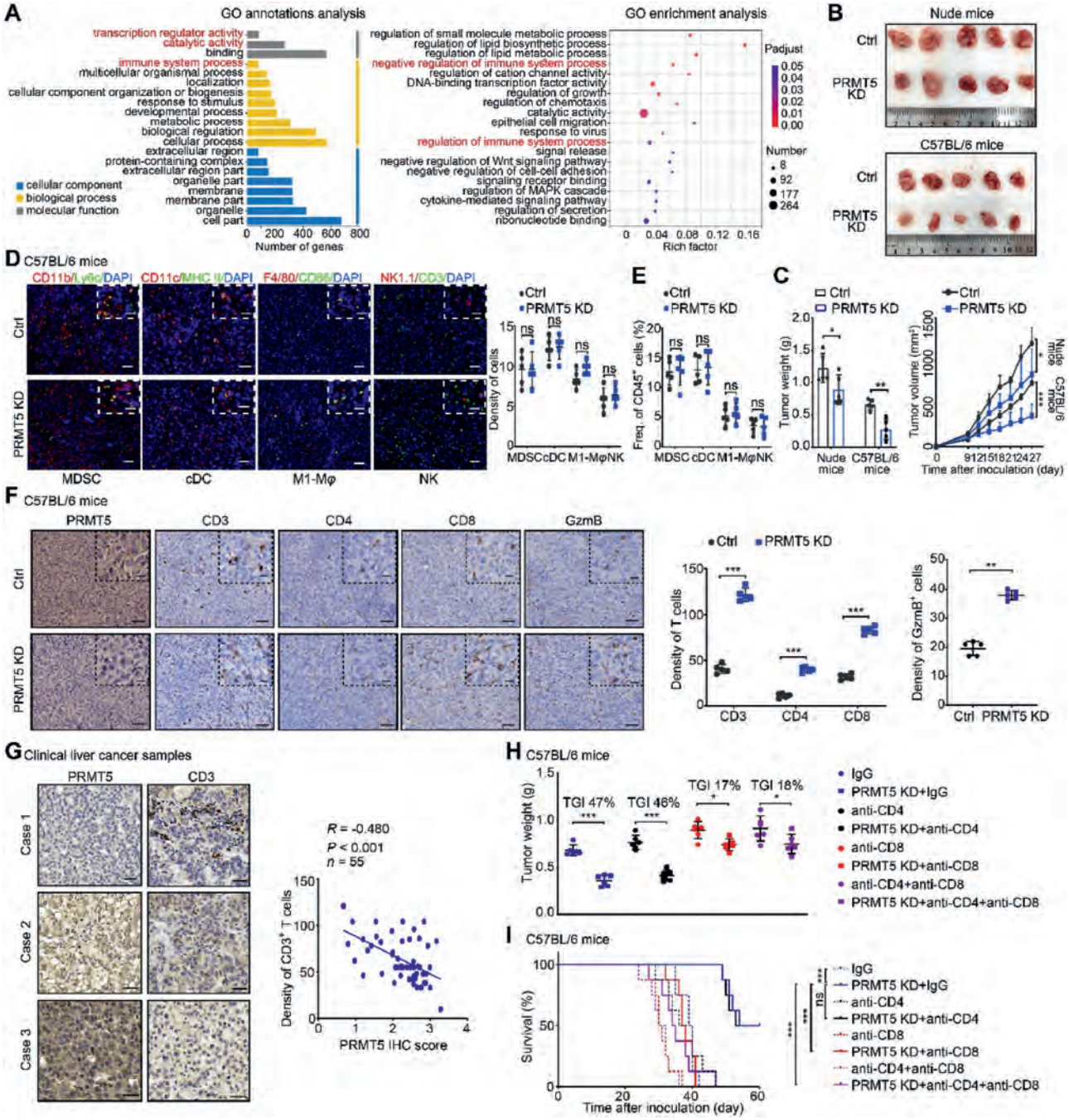

Figure 1 PRMT5 disruption promotes $CD8^+$ T-cell-mediated antitumor immunity suppressing liver cancer growth. (A) GO analysis of differentially expressed genes between control and PRMT5-KD HepG2 cells, as determined by RNA-seq ($n = 3$). (B) Tumor appearance in nude and C57BL/6 mice post-inoculation with Hepa1-6 (Ctrl) or Hepa1-6 (PRMT5 KD) cells ($n = 5$). (C) Excised tumor weights (left) and tumor volume changes (right) for each group, with volume measurements every 3 days ($n = 5$). (D) Representative immunofluorescence images and quantitative analysis of MDSC ($CD11b^+$ $Ly6c^+$), cDC ($CD11c^+$ $MHCII^+$), M1-Mϕ ($F4/80^+$ $CD86^+$), and NK cell ($NK1.1^+$ $CD3^-$) in Ctrl and PRMT5-KD tumors of C57BL/6 mice. Scale bar, 50 μm or 20 μm. (E) Frequencies of MDSCs ($CD45^+$ $CD11b^+$ $Gr1^+$), cDCs ($CD45^+$ $CD3^-$ $NK1.1^-CD11c^+$ $MHCII^+$), M1-Mϕs ($CD45^+$ $CD11b^+$ $F4/80^+$ $CD86^+$), and NK cells ($CD45^+$ $CD3^-$ $NK1.1^+$) within $CD45^+$ cells in Ctrl and PRMT5-KD tumors from C57BL/6 mice, as quantified by flow cytometry. (F) Representative immunohistochemistry (IHC) images and quantification of PRMT5, $CD3^+$, $CD4^+$, $CD8^+$, and $GzmB^+$ T cells in tumor tissues of C57BL/6 mice ($n = 5$). Scale bar, 50 μm or 20 μm. (G) Representative IHC images and correlation analysis of PRMT5 levels and $CD3^+$ T cells in clinical liver cancer samples ($n = 55$). Scale bar, 50 μm. (H) Tumor weights of C57BL/6 mice across eight groups: IgG, PRMT5 KD + IgG, anti-CD4, PRMT5 KD + anti-CD4, anti-CD8, PRMT5 KD + anti-CD8, anti-CD4 + anti-CD8, and PRMT5 KD + anti-CD4 + anti-CD8 ($n = 6$). (I) Survival analysis across 8 groups ($n = 8$). $^*P < 0.05$, $^{**}P < 0.01$, $^{***}P < 0.001$; ns: no significance. GO: Gene Ontology, KD: knockdown, MDSC: myeloid-derived suppressor cell, cDC: conventional dendritic cell, M1-Mϕ: M1 macrophage, NK: natural killer, GzmB: granzyme B, TGI: tumor growth inhibition value.

dendritic cells (cDCs), pro-inflammatory M1 macrophages (M1-Mϕs), and NK cells between PRMT5-KD tumors and controls. Subsequently, we observed that PRMT5 KD markedly enhanced the infiltration and activation of T cells in the tumor tissues from C57BL/6 mice relative to controls (Fig. 1F). Additionally, flow cytometry showed comparable regulatory T cells (Treg) frequencies between PRMT5-KD and control tumor tissues (Fig. S1H). Furthermore, IHC analysis revealed an inverse correlation between PRMT5 levels and the presence of $CD3^+$ T cells in clinical liver cancer samples (Fig. 1G). The above results confirm that PRMT5 potentially impairs T-cell-mediated antitumor immunity.

To specifically assess the contribution of different T-cell subsets in PRMT5 disruption-mediated tumor growth suppression, we monitored the growth of PRMT5-KD Hepa1-6 tumors following the depletion of $CD4^+$ or $CD8^+$ T cells, or both simultaneously. In mice treated with IgG or those with only anti-CD4, PRMT5 KD significantly attenuated tumor growth (TGI: 47% and 46%, respectively; Fig. 1H). However, administering neutralizing antibodies against either solely $CD8^+$ T cells or both $CD4^+$ and $CD8^+$ T cells weakened the inhibitory effect of PRMT5 KD on tumor growth (TGI: 17% and 18%, respectively; Fig. 1H). Moreover, upon depletion of $CD8^+$ T cells, the survival advantage conferred by PRMT5 KD was notably reduced, while the depletion of $CD4^+$ T cells showed no such impact (Fig. 1I). This suggests that the survival benefits derived from PRMT5 KD are mediated through the activation of $CD8^+$ T cells. These findings demonstrate that PRMT5 knockdown boosts $CD8^+$ T-cell-mediated antitumor immunity, thereby suppressing liver cancer growth.

3.2. PRMT5 inhibition enhances $CD8^+$ T-cell antitumor immunity via downregulating FGL1 expression in vivo and in vitro

We next investigated whether tumor-derived PRMT5 directly impairs $CD8^+$ T cell effector functions. Hepa1-6-OVA tumor cells were co-cultured with OT-1 $CD8^+$ T cells. Compared to the control, OT-1 T cells co-cultured with PRMT5-KD tumor cells exhibited significantly increased granzyme B (GzmB) production (Fig. 2A) and enhanced tumor cell-killing activity (Fig. 2B). Notably, CD3/CD28-activated $CD8^+$ T cells also displayed enhanced cytotoxic function when co-cultured with PRMT5-KD Hepa1-6 cells lacking OVA expression (Fig. 2C and D), demonstrating that this effect is independent of antigen-specific signaling. These findings indicate that tumor-derived PRMT5 suppresses $CD8^+$ T cell cytotoxicity, primarily through a mechanism unrelated to antigen recognition.

Subsequently, we explored the underlying mechanism through which PRMT5 suppressed $CD8^+$ T-cell antitumor immunity in liver cancer. Prior studies indicate that PRMT5 can modulate tumor immunity through either upregulating or downregulating the expression of PD-L1[7,8]. However, PD-L1 levels remained unchanged after siPRMT5 treatment in HepG2 and Huh7 cells (Supporting Information Fig. S2A), suggesting that PRMT5 is not involved in PD-L1-mediated immune escape in liver cancer. The heatmap displayed the top 10 immune-related DEGs following PRMT5 KD (Fig. 2E). qPCR analysis verified the expression of these genes in HepG2 and Huh7 cells treated with PRMT5 KD (Fig. S2B). Among these, FGL1, an inhibitory immune checkpoint, exhibited the most significant change (Fig. S2B). Previous studies have demonstrated that FGL1 inhibits T-cell activation and expansion within the tumor microenvironment, playing a crucial role in tumor immune evasion[19]. Thus, we hypothesized that FGL1 could be a potential critical downstream target molecule of PRMT5. To verify this hypothesis, we first knocked down PRMT5 in HepG2 and Huh7 cells, resulting in a concentration-dependent reduction in both mRNA and protein levels of FGL1 (Fig. 2F and Fig. S2C). Similarly, ELISA analysis revealed that intervening with PRMT5 also affects the levels of secreted FGL1 protein, indicating a consistent trend in changes (Fig. S2D). Moreover, PRMT5 inhibitor GSK591 suppressed the PRMT5 methyltransferase activity (H4R3me2s, histone H4 arginine 3 symmetric dimethylation; Rme2sy/sDMA, symmetric dimethylation of arginine residues), leading to a dose-dependent decrease in FGL1 mRNA and protein levels in HepG2 and Huh7 cells (Fig. 2G and Fig. S2E). Consistently, ELISA analysis showed that GSK591 also dose-dependently reduced the levels of secreted FGL1 protein in HepG2 and Huh7 cells (Fig. S2F). These findings were validated in Hepa1-6 cells (Fig. S2G). Importantly, qPCR analysis of clinical liver cancer samples demonstrated a positive correlation between *PRMT5* and *FGL1* mRNA levels, which was further confirmed by IHC analysis at the protein level (Fig. 2H). Collectively, these results indicate that PRMT5 can regulate the expression of FGL1.

To delve into the role of FGL1 in PRMT5-mediated $CD8^+$ T-cell function, HepG2 or Huh7 cells were co-cultured with $CD8^+$ T cells. The siFGL1#2 showed the best knockdown efficiency, which was selected for subsequent experiments (Fig. S2H). Our data revealed that, akin to FGL1-KD, co-culturing with PRMT5-KD liver cancer cells notably promoted $CD8^+$ T-cell proliferation and activation, evidenced by increased Ki67 (Fig. 2I) and GzmB ratios (Fig. 2J), along with heightened IL-2 secretion (Fig. 2K). However, overexpressing FGL1 reversed these effects (Fig. 2I−K). Similarly, co-culturing with PRMT5 or FGL1-KD liver cancer cells enhanced $CD8^+$ T-cell-mediated tumor cell-killing effect compared to the control group; overexpressing FGL1 reversed these effects (Fig. 2L). Additionally, cell migration experiments revealed that targeting PRMT5 or FGL1 in HepG2 and Huh7 cells does not impact the migratory ability of $CD8^+$ T cells (Fig. S2I). All these results indicate that FGL1 serves as a crucial mediator of PRMT5-induced $CD8^+$ T-cell function suppression in liver cancer.

To determine whether PRMT5 inhibition-mediated enhancement of the $CD8^+$ T immune response was dependent on FGL1 *in vivo*, Ctrl, PRMT5-KD, FGL1-KD and PRMT5-KD + FGL1-OE H22 cells were subcutaneously inoculated into BALB/c mice. The findings indicated that knocking down either FGL1 or PRMT5 resulted in reduced FGL1 protein levels within tumor tissues (Fig. S2J). Similar to FGL1-KD effects, PRMT5 KD increased the infiltrated $CD8^+$ T-cell number and enhanced intratumoral $CD8^+$ T-cell activation compared to the control group, which reduced tumor growth; however, FGL1 OE reversed these effects (Fig. 2M−O, Fig. S2K). Furthermore, H22 cells with PRMT5 or FGL1 KD exhibited similar proliferation rates as the control group *in vitro* (Fig. S2L), suggesting that neither PRMT5 nor FGL1 affect the intrinsic proliferation capacity of H22 cells. These results suggest that PRMT5 inhibition could enhance $CD8^+$ T-cell antitumor immunity to mitigate liver cancer progression by downregulating FGL1 expression.

In summary, PRMT5 inhibition enhances the $CD8^+$ T-cell antitumor immune response by diminishing FGL1 expression levels both *in vivo* and *in vitro*.

3.3. TCF12 transcriptionally upregulates FGL1 expression in liver cancer

As a methyltransferase, PRMT5 can enhance transcription factor binding to DNA *via* arginine symmetric dimethylation

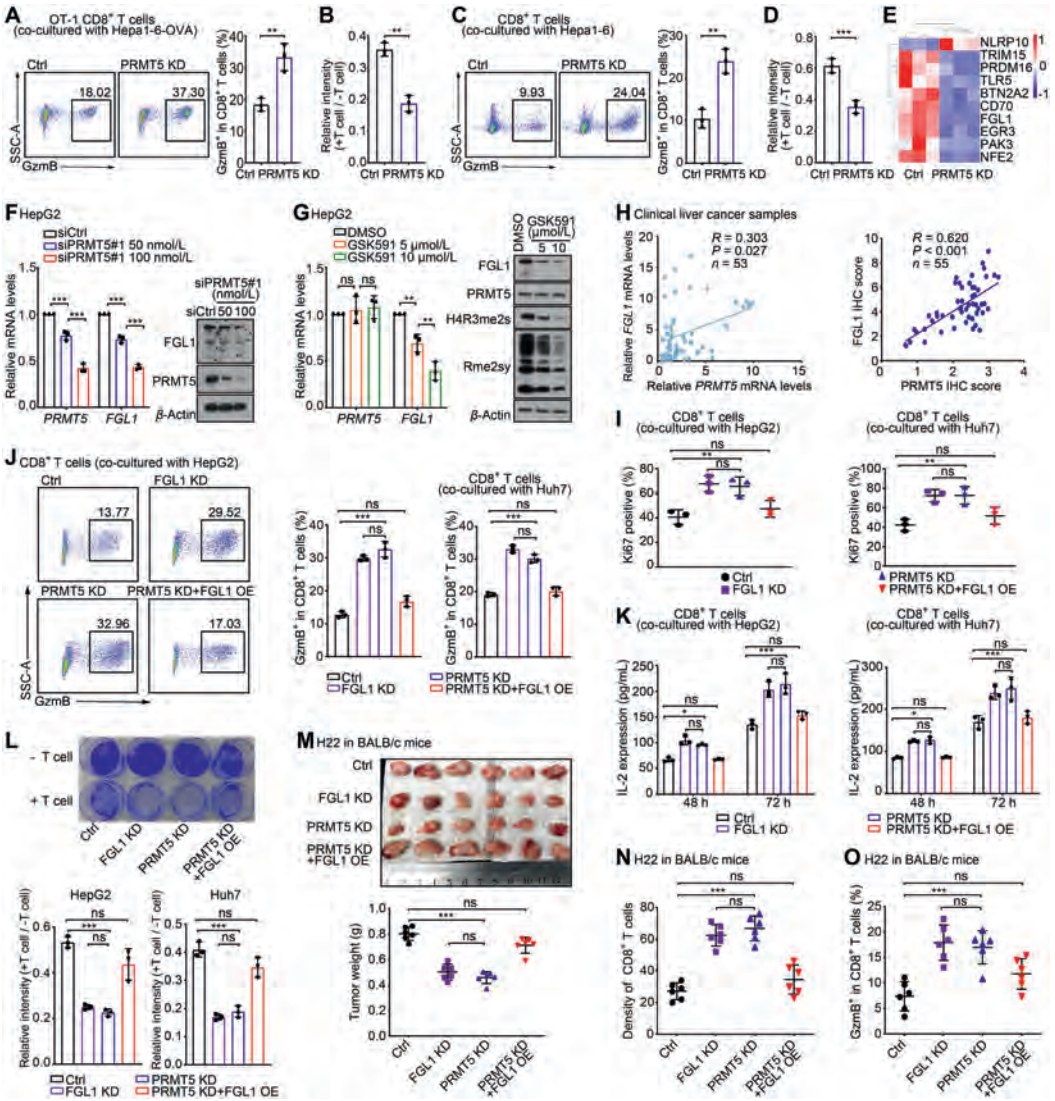

Figure 2 PRMT5 inhibition enhances CD8$^+$ T-cell antitumor immunity *via* downregulating FGL1 expression *in vivo* and *in vitro*. (A) OT-1 CD8$^+$ T cells were co-cultured with Hepa1-6-OVA cells treated with Ctrl or PRMT5 KD for 48 h. The proportion of GzmB$^+$ cells within CD8$^+$ T cells was quantified by flow cytometry. (B) T-cell-mediated tumor cell killing assays were performed by co-culturing OT-1 CD8$^+$ T cells with the indicated Hepa1-6-OVA cells for 24 h, followed by quantification of surviving cell intensities. (C) CD8$^+$ T cells were co-cultured with Hepa1-6 cells treated with Ctrl or PRMT5 KD for 48 h. The proportion of GzmB$^+$ cells within CD8$^+$ T cells was quantified by flow cytometry. (D) T-cell-mediated tumor cell killing assays were performed by co-culturing CD8$^+$ T cells with the indicated Hepa1-6 cells for 72 h, followed by quantification of surviving cell intensities. (E) Heatmap displaying top 10 DEGs among Ctrl and PRMT5 KD treated HepG2 cells. (F) The mRNA and protein levels of PRMT5 and FGL1 in HepG2 cells treated with siCtrl and siPRMT5 (50 or 100 nmol/L). (G) The mRNA levels of *PRMT5* and *FGL1* in HepG2 cells treated with DMSO, GSK591 (5 μmol/L), or GSK591 (10 μmol/L), alongside the protein levels of FGL1, PRMT5, H4R3me2s, and Rme2sy in each treatment group. (H) Correlation analysis of mRNA ($n = 53$) and protein levels ($n = 55$) between PRMT5 and FGL1 in human liver cancer tissues, using Pearson's correlation coefficient. (I–K) CD8$^+$ T cells were co-cultured with HepG2 or Huh7 cells treated with Ctrl, FGL1 KD, PRMT5 KD, or PRMT5 KD + FGL1 OE. (I, J) Flow cytometry analysis of the proportions of Ki67$^+$ CD8$^+$ T cells (I) and GzmB$^+$ CD8$^+$ T cells (J). (K) IL-2 expression in the co-culture supernatant was measured after 48 and 72 h using ELISA. (L) T-cell-mediated tumor cell killing assays conducted by co-culturing CD8$^+$ T cells with either HepG2 or Huh7 cells for 72 h. Representative images of surviving tumor cells visualized with crystal violet staining (upper), and quantification of surviving cell intensities (lower). (M) Tumor appearance and weights in BALB/c mice following inoculation with Ctrl, FGL1-KD, PRMT5-KD, and PRMT5-KD + FGL1-OE H22 cells ($n = 6$). (N) Intratumoral CD8$^+$ T-cell density across various groups, as detected by IHC staining ($n = 6$). (O) Intratumoral proportions of GzmB$^+$ CD8$^+$ T cells across various groups, as detected by flow cytometry. *$P < 0.05$, **$P < 0.01$, ***$P < 0.001$; ns: no significance. KD: knockdown, OE: overexpression, GzmB: granzyme B.

modification, thereby promoting transcriptional activation of target genes[27]. Previous experiments have shown that the PRMT5 methyltransferase inhibitor, GSK591, could decrease the levels of FGL1 mRNA and protein (Fig. 2G, Fig. S2E and S2F). Based on these findings, we hypothesized that PRMT5 could regulate FGL1 by methylation of transcription factors. Then, we sought to identify the PRMT5-modified transcription factors that targeted FGL1 in tumor cells. The Toolkit, JASPAR, and hTFtarget online databases identified TCF12 as a top candidate transcription factor involved in the regulation of FGL1 (Supporting Information Fig. S3A). Subsequently, siRNAs were used to knockdown TCF12, and siTCF12#1 had the best knockdown efficiency (Fig. S3B). We performed TCF12 knockdown and overexpression experiments in HepG2 and Huh7 cells. The results showed that the changes of FGL1, both at mRNA and protein levels, correlated with the alterations of TCF12 in HepG2 and Huh7 cells (Fig. 3A and B, Fig. S3C and S3D). Subsequently, TCF12-KO Hepa1-6 cells were constructed (Fig. S3E). Similar effects were observed in mouse liver cancer cells (Fig. S3F and S3G), thus suggesting a conserved role of TCF12 in upregulating FGL1 in liver cancer across species.

To elucidate the transcriptional regulation mechanism, we investigated the binding sites of TCF12 within the FGL1 promoter region. TCF12-KO HepG2 cells were established (Fig. S3H). By employing dual luciferase reporter assays with full-length and segmented FGL1 promoter constructs in TCF12-KO HepG2 and control cells, we identified the −1460/−920 fragment as the core region of the FGL1 promoter essential for its activity (Fig. 3C). Furthermore, the luciferase activities of constructs pGL3-2101 and pGL3-1561 were significantly enhanced by TCF12 overexpression, whereas constructs pGL3-1021, pGL3-661, and pGL3-391 showed no change (Fig. 3D). These results confirm the specific binding of TCF12 to the FGL1 promoter and its regulatory impact on FGL1 transcription.

TCF12, as an E-protein with a basic-helix-loop-helix (bHLH) domain, can recognize and bind to E-box sites (CANNTG)[28]. JASPAR database predicted the sequence logo representing DNA sequences bound by the TCF12 (Fig. S3I) and identified three potential TCF12 binding sites in the FGL1 promoter (Fig. S3J). ChIP demonstrated that TCF12 was recruited only to the promoter regions containing binding site 2 (Fig. 3E). We conducted an in-depth analysis of TCF12 expression in clinical liver cancer samples obtained from our center. Results revealed that compared with adjacent tissues, the mRNA (Fig. S3K) and protein levels (Fig. S1B) of TCF12 were notably upregulated in tumor tissues. Furthermore, *TCF12* and *FGL1* mRNA levels exhibited a positive correlation in these clinical samples (Fig. 3F), which was corroborated by IHC staining (Fig. 3G). Collectively, these results indicate that TCF12 transcriptionally upregulates FGL1 expression in liver cancer.

3.4. PRMT5 catalyzes symmetric dimethylation of TCF12 at the R554 residue

We further delved into the mechanism by which PRMT5 modifies TCF12 to upregulate FGL1 in liver cancer. The bioinformatics analysis revealed a potential interaction between PRMT5 and TCF12 (Fig. 4A). This interaction was further substantiated through confocal microscopy, which depicted nuclear co-localization of PRMT5 and TCF12 within HepG2 cells (Fig. 4B). Moreover, GST-pulldown assays confirmed a direct binding between PRMT5 and TCF12 *in vitro* (Fig. 4C). Consistently, TCF12 CoIP assays confirmed that endogenous TCF12 interacts with PRMT5 in both human and mouse liver cancer cell lines (Fig. 4D and Supporting Information Fig. S4A). Collectively, these results confirm the interaction between PRMT5 and TCF12.

Subsequent immunoprecipitation (IP) assays demonstrated that TCF12 undergoes symmetric dimethylarginine modifications, which are diminished upon PRMT5 KD in both HepG2 and Huh7 cells (Fig. 4E), indicating PRMT5's critical role in TCF12's symmetric dimethylation. In mammals, the enzymes responsible for symmetric dimethylarginine modification are PRMT5 and PRMT9[29]. However, PRMT9 KD did not reduce TCF12's Rme2sy levels in the systems (Fig. 4E), indicating that PRMT9 does not participate in the events. Furthermore, PRMT5 inhibitors, specifically GSK591 and HLCL61, attenuated Rme2sy levels on TCF12 and correspondingly decreased FGL1 expression in human and mouse liver cancer cells, with GSK591 showing superior effects (Fig. 4F and Fig. S4B). CoIP assays validated the PRMT5-TCF12 interaction, and the overexpression of PRMT5 significantly enhanced TCF12's Rme2sy levels in 293T cells (Fig. 4G), further substantiating PRMT5's critical role in this dimethylation process.

As the primary arginine symmetric dimethylase, PRMT5 preferentially modifies RG/GR/RGG motifs enriched in arginine (R) and glycine (G)[30,31]. we analyzed all arginine residues in TCF12 containing RG/GR/RGG motifs and discerned 8 analogous sequences: R54GG, R74G, R114G, R299G, R326G, R503GG, R554G and GR602. To identify the exact methylation site, we constructed two arginine-to-lysine (K) composite mutants (Fig. S4C): 2RK (R54K, R503K) and 6RK (R74K, R114K, R299K, R326K, R554K, R602K). Methylation analysis showed that the 6RK mutant notably diminished the PRMT5-induced Rme2sy signal in 293T cells (Fig. 4H-left), indicating that the potential methylation site may be located within these residues. Thus, we further analyzed these 6 sites, and found that R554 residue was adjacent to the key region of TCF12 transcription factor binding to E-box promoter: the bHLH domain, identifying it as a potential catalytic site of PRMT5. To validate this hypothesis, we constructed single mutant R554K and composite mutant 5RK (R74K, R114K, R299K, R326K, R602K). Strikingly, R554K significantly reduced the PRMT5-induced Rme2sy signal, while 5RK failed to work (Fig. 4H-right), suggesting that R554 is the catalytic site of PRMT5. Sequence alignment showed the conservation of this R554 site across species (Fig. S4D). Furthermore, we purified PRMT5 protein along with TCF12 WT and the TCF12 R554K mutant proteins (Fig. 4I). The *in vitro* methylation assay demonstrated that TCF12 wild type (WT), but not the R554K mutant, could be methylated by PRMT5 (Fig. 4J), which aligns with the results from the IP experiment. Taken together, these findings indicate that PRMT5 catalyzes arginine symmetric dimethylation of TCF12 at the R554 residue.

3.5. TCF12-R554 methylation promotes FGL1 transcriptional activation and inhibits $CD8^+$ T-cell antitumor immunity

Numerous studies have shown that members of the PRMTs family can be co-recruited with transcription factors to the promoter regions of their target genes[32-34]. Our research also verified that PRMT5 can interact with TCF12 within the nucleus. Subsequent Re-ChIP experiments have validated that PRMT5 was recruited to the FGL1 promoter, particularly associating with TCF12 at its specific binding region on the FGL1 promoter (Fig. 5A).

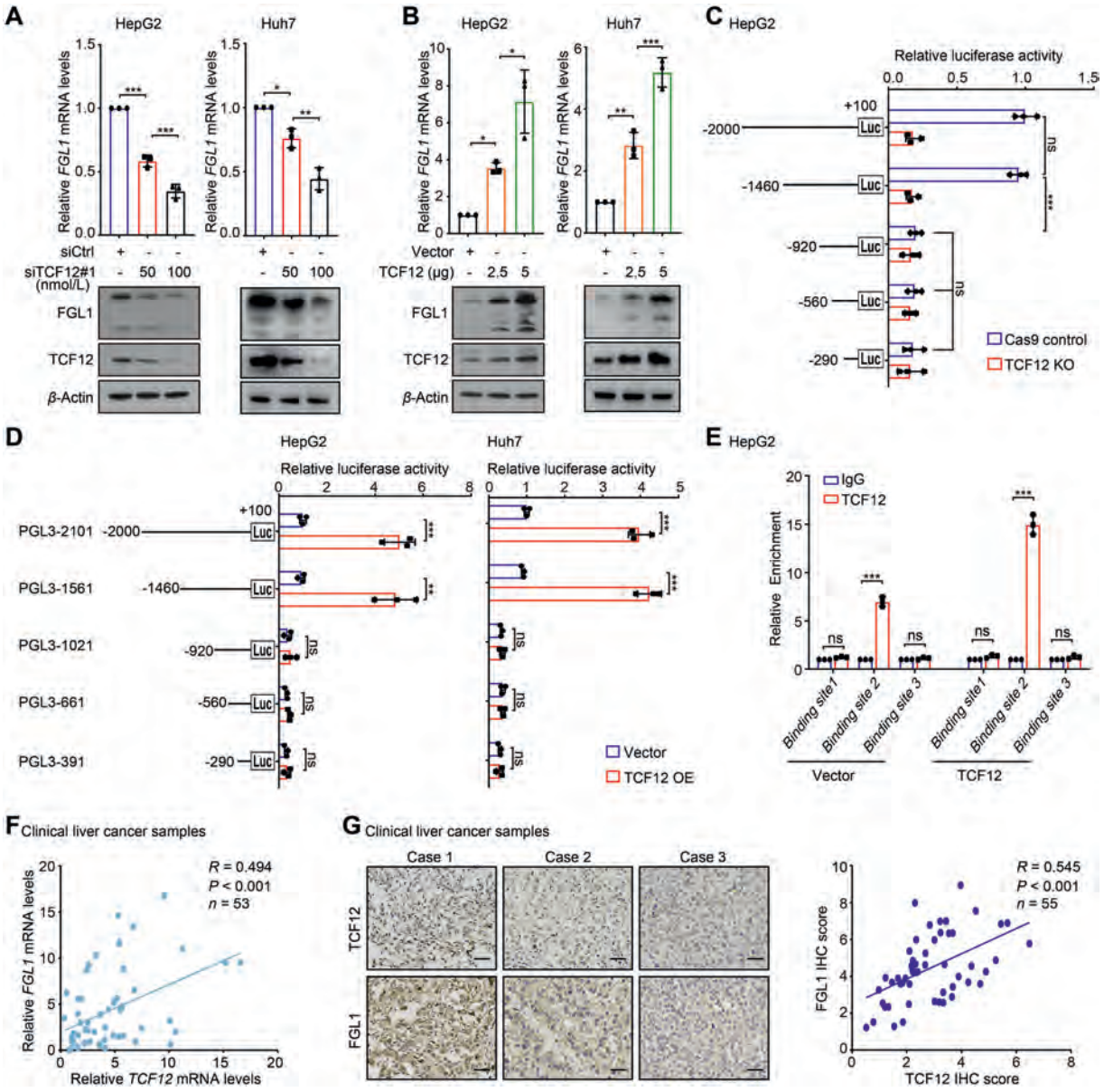

Figure 3 TCF12 transcriptionally upregulates FGL1 expression in liver cancer. (A, B) Protein and mRNA levels of FGL1 in HepG2 and Huh7 cells following TCF12 knockdown (A) and overexpression (B). (C) Luciferase activities of FGL1 promoter reporter vectors in Cas9 control and TCF12-KO HepG2 cells. (D) Luciferase activities of FGL1 promoter reporter vectors in HepG2 and Huh7 cells transfected with either Flag-vector or Flag-TCF12 plasmids. (E) ChIP analysis of TCF12 binding to FGL1 promoter in HepG2 cells. Different regions of the FGL1 promoter containing different putative TCF12 binding sites are shown in Fig. S3J. (F) Correlation analysis of *TCF12* and *FGL1* mRNA levels in human liver cancer tissues using Pearson's correlation coefficient ($n = 53$). (G) Representative IHC images and correlation analysis of TCF12 and FGL1 protein levels in human liver cancer tissues, using Pearson's correlation coefficient ($n = 55$). Scale bar, 50 μm. $^{*}P < 0.05$, $^{**}P < 0.01$, $^{***}P < 0.001$; ns: no significance. KO: knockout, WT: wide type, OE: overexpression.

Furthermore, the knockdown of either PRMT5 or TCF12 resulted in decreased recruitment to the FGL1 promoter region (Fig. 5B), supporting that PRMT5 and TCF12 are interdependently occupied on the FGL1 promoter in tumor cells. PRMT5 has been demonstrated to enhance the binding affinity of transcription factors to promoter region DNA *via* methylation[27]. In prior experiments, we ascertained that PRMT5 methylates TCF12, the transcription factor for FGL1, at the R554 residue (Fig. 4H–J). Based on this finding, we further investigated whether this methylation at R554 is essential for TCF12's binding affinity to the FGL1 promoter and thereby affects the transcriptional regulation of FGL1. In TCF12-KO HepG2 cells transfected with TCF12 (WT), TCF12 (R554K) or PRMT5 plasmid alone or in combination, ChIP experiments showed that recruitment of TCF12 (WT) to the FGL1 promoter region was significantly higher than that of TCF12 (R554K), and PRMT5 overexpression enhanced TCF12 (WT) binding but not TCF12 (R554K) (Fig. 5C), suggesting that PRMT5 enhances TCF12 recruitment to the FGL1 promoter by methylation of TCF12 R554 residue. Consistent with ChIP assay, transfection of TCF12 (WT) could induce TCF12 symmetric dimethylarginine and upregulated FGL1 expression in TCF12-KO HepG2 cells, but nor TCF12 (R554K) (Fig. 5D). Comparable results were observed

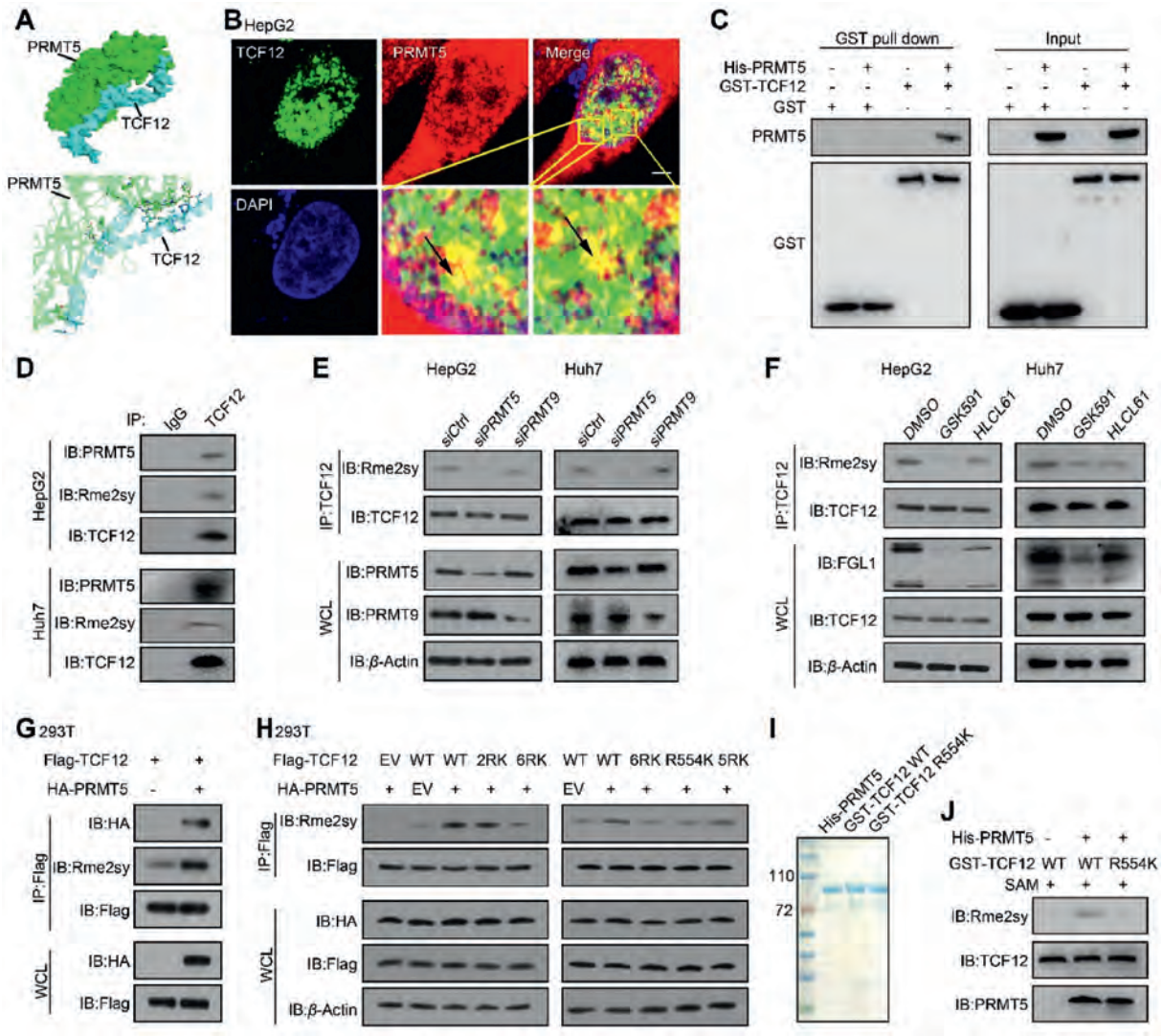

Figure 4 PRMT5 catalyzes symmetric dimethylation of TCF12 at the R554 residue. (A) Diagram illustrating the binding of PRMT5 with TCF12 (upper). Residues around the protein−protein interaction interface form numerous hydrophobic interactions (lower). (B) Confocal microscopy showed the co-localization of PRMT5 and TCF12 (indicated by black arrows). Scale bar, 2 μm. (C) GST pulldown assay analyzing the direct binding between PRMT5 and TCF12 proteins. (D) Co-immunoprecipitation analysis was conducted to detect the interaction between endogenous TCF12 with PRMT5, and the Rme2sy levels of TCF12 in HepG2 and Huh7 cells. (E) Immunoprecipitation analysis of TCF12 methylation in HepG2 and Huh7 cells treated with siCtrl, siPRMT5 or siPRMT9. (F) Immunoprecipitation analysis of TCF12 methylation in HepG2 and Huh7 cells treated with DMSO, GSK591 or HLCL61. (G) Immunoprecipitation analysis was performed to detect the methylation of ectopic TCF12 in 293T cells transfected with Flag-TCF12, either alone or in conjunction with HA-PRMT5 transfection. (H) Immunoprecipitation analysis of ectopic TCF12 methylation in 293T cells transfected with Flag-tagged TCF12 wild type or composite mutants, with or without HA-PRMT5. (I) Coomassie Brilliant Blue staining of purified His-tagged PRMT5 protein, GST-tagged TCF12 wild type, and GST-tagged TCF12 R554K mutant proteins. (J) *In vitro* methylation analysis of GST-tagged TCF12 wild type and GST-tagged TCF12 R554K mutant proteins by His-tagged PRMT5 protein. EV: empty vector, WT: wide type, RK: arginine to lysine substitution, SAM: *S*-adenosylmethionine.

in TCF12-KO Hepa1-6 cells, and GSK591 treatment could attenuate the FGL1 upregulation induced by TCF12 (WT) (Fig. 5E). TCF12 (WT) but not TCF12 (R554K) could rescue the diminished supernatant FGL1 levels following TCF12 KO (Fig. 5F). All results demonstrated that PRMT5-mediated methylation at TCF12 R554 residue enhances its recruitment to FGL1 promoter region, consequently elevating FGL1 expression.

We next investigated the impact of TCF12-R554 methylation on $CD8^+$ T cell antitumor immunity. Co-culture experiments of HepG2 and $CD8^+$ T cells *in vitro* demonstrated that TCF12-KO HepG2 cells increased $CD8^+$ T-cell cytotoxicity (Fig. 5G) and IL-2 production (Fig. 5H). Conversely, reintroducing TCF12 (WT) reversed these enhancements, while the R554K mutant did not (Fig. 5G and H), suggesting that TCF12 R554 methylation upregulates FGL1 expression to attenuate $CD8^+$ T-cell antitumor immunity.

Subsequently, we used an immunocompetent liver cancer mouse model to examine the effect of TCF12-R554 methylation regulating FGL1 on $CD8^+$ T-cell antitumor immunity *in vivo*. Our data indicate that TCF12 KO reduced FGL1 protein levels in tumor tissues, and while TCF12 (WT) restoration could reverse the reduction in FGL1 levels, TCF12 (R554K) did not achieve this

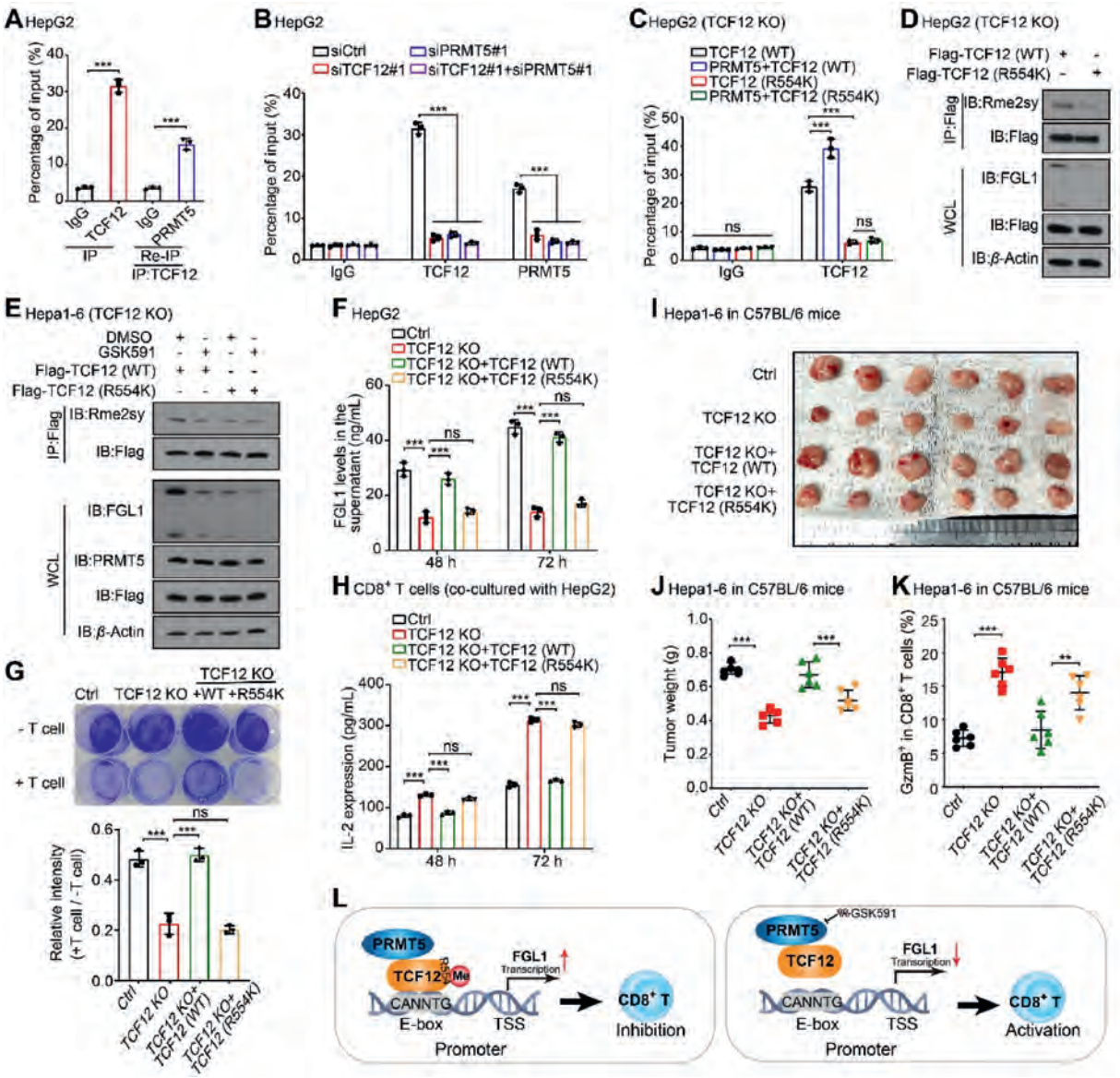

Figure 5 TCF12-R554 methylation promotes FGL1 transcriptional activation and inhibits $CD8^+$ T-cell antitumor immunity. (A) ChIP/Re-ChIP analysis of TCF12 and PRMT5 complex occupancy on the FGL1 promoter region in HepG2 cells. (B) ChIP analysis of TCF12 and PRMT5 occupancy on the FGL1 promoter region in HepG2 cells treated with siPRMT5, siTCF12, alone or in combination. (C) ChIP analysis of ectopic TCF12 occupancy on the FGL1 promoter region transfected with TCF12 (WT), PRMT5, and TCF12 (R554K) individually or simultaneously. (D) Immunoprecipitation analysis of ectopic TCF12 methylation and FGL1 protein levels in HepG2 (TCF12 KO) cells transfected with Flag-tagged TCF12 (WT) or TCF12 (R554K). (E) Immunoprecipitation was used to assess the ectopic TCF12 methylation and FGL1 protein levels in the specified TCF12-KO Hepa1-6 cells. (F) In HepG2 (TCF12 KO) cells transfected with TCF12 (WT) or TCF12 (R554K), secreted FGL1 protein levels in the supernatant were assessed after 48 and 72 h using ELISA. (G) T-cell-mediated tumor cell killing assays were conducted by co-culturing $CD8^+$ T cells with specified HepG2 cells for 72 h. Representative images of surviving tumor cells visualized with crystal violet staining, and quantification of surviving cell intensities. (H) After co-culturing $CD8^+$ T cells with the indicated HepG2 cells, IL-2 expression levels in the co-culture supernatant were measured at 48 h and 72 h using ELISA. (I, J) Tumor appearance (I) and weights (J) in C57BL/6 mice following inoculation with Ctrl, TCF12 KO, TCF12 KO + TCF12 (WT), and TCF12 KO + TCF12 (R554K) Hepa1-6 cells ($n = 6$). (K) Intratumoral proportions of $GzmB^+$ $CD8^+$ T cells across various groups, as detected by flow cytometry. (L) A model illustrating how PRMT5-catalyzed TCF12 methylation at R554 modulates FGL1 expression to attenuate $CD8^+$ T-cell activity. $^{**}P < 0.01$, $^{***}P < 0.001$; ns: no significance. KO: knockout, WT: wide type, IL-2: interleukin 2, RK: arginine to lysine substitution, GzmB: granzyme B, TSS: transcription start site, Me: arginine symmetric demethylation modification.

effect (Supporting Information Fig. S5A). TCF12 depletion significantly enhanced intratumoral $CD8^+$ T-cell activation indicated by GzmB and inhibited tumor growth compared to the control tumors (Fig. 5I–K). Notably, an increased proportion of activated $CD8^+$ T cells in tumors expressing TCF12-R554K compared to those with TCF12-WT, which attenuated tumor growth (Fig. 5I–K). However, no growth suppression was observed in cultured cells (Fig. S5B), aligning with the notion that

these factors primarily mediate immune recognition of the tumor *in vivo*. These results suggest that TCF12-R554 methylation deficiency enhances $CD8^+$ T-cell activation by reducing FGL1 expression, leading to tumor growth inhibition.

In conclusion, our data support that TCF12 promotes FGL1 expression *via* PRMT5-mediated methylation at the R554 residue, thereby reducing $CD8^+$ T-cell antitumor immune response (Fig. 5L).

3.6. PRMT5 suppresses $CD8^+$ T-cell activity via TCF12/FGL1 axis in vitro

Next, we further verified the regulatory relationship within the PRMT5/TCF12/FGL1 axis and its effects on $CD8^+$ T-cell activity. In both HepG2 and Huh7 cell lines, PRMT5 overexpression increased FGL1 protein levels (Fig. 6A). However, TCF12 depletion negated this effect in these cells (Fig. 6A). Consistent results were observed when measuring the secreted FGL1 levels in the supernatant of HepG2 and Huh7 cells (Fig. 6B), supporting that PRMT5 promotes FGL1 expression through TCF12. In co-culture systems with liver cancer cells and $CD8^+$ T cells, overexpression of PRMT5 in HepG2 or Huh7 cells significantly reduced the proportion of activated $CD8^+$ T cells indicated by GzmB, perforin, and IL-2 (Fig. 6C−E). The depletion of TCF12 reversed these suppressive effects on $CD8^+$ T cells (Fig. 6C−E), illustrating that PRMT5 inhibits $CD8^+$ T-cell function through TCF12/FGL1 axis (Fig. 6F).

3.7. PRMT5 inhibitor boosts PD-L1 mAb sensitivity in liver cancer immunotherapy

The FGL1−LAG3 pathway represents an independent mechanism of tumor immune evasion, and blocking this interaction can synergize with anti-PD-L1 therapy[19]. Based on that PRMT5 disruption could activate antitumor immunity *via* decreasing FGL1 in tumor cells, we explored a combination therapy using GSK591 and PD-L1 mAb in subcutaneous liver cancer models (Fig. 7A). The results showed that the combined treatment of GSK591 and PD-L1 mAb markedly inhibited tumor growth, superior to monotherapy (Fig. 7B−D). Further IHC analysis revealed that GSK591 decreased FGL1 expression in tumors from C57BL/6 mice (Fig. 7E). Compared with control group, tumor-infiltrated $CD8^+$ T-cell counts were increased in groups treated with either GSK591 alone or PD-L1 mAb individually (Fig. 7E). Flow cytometry analysis revealed that both GSK591 and PD-L1 mAb monotherapy increased the proportion of $GzmB^+$ $CD8^+$ T cells (Fig. 7F). Notably, the combination therapy significantly promoted intratumoral $CD8^+$ T-cell expansion and activation compared to monotherapy (Fig. 7E and F), resulting in augmented antitumor immunity. However, no significant differences were observed in draining lymph nodes regarding $GzmB^+$ $CD8^+$ T cells among the 4 groups (Fig. 7G), implying that the primary effect of GSK591 and PD-L1 mAb enhances the $CD8^+$ T-cell antitumor immune response only locally, within the tumor microenvironment. Importantly, the combination therapy conferred a survival advantage compared to monotherapy (Fig. 7H). Consequently, we conclude that the PRMT5 inhibitor GSK591 significantly enhances the efficacy of PD-L1 mAb in liver cancer immunotherapy.

4. Discussion

PRMT5 has been recognized as a critical regulator of tumorigenesis and progression in liver cancer[9,10,23]. Previous research has mainly focused on PRMT5's role in driving intrinsic alterations within tumor cells. However, the impact of PRMT5 on the liver cancer immune microenvironment remains unclear. In this study, we explored the potential effects of PRMT5 on liver cancer antitumor immunity and response to immunotherapy.

In this study, inhibiting PRMT5 was shown to suppress liver cancer growth in immunodeficient mice, indicating PRMT5's intrinsic regulation of tumor cells, consistent with prior research[35-37]. Crucially, by comparing the results from experiments with immunocompetent and immunodeficient mice, we uncovered the vital role of PRMT5 derived from liver cancer cells in modulating antitumor immune response. Moreover, by conducting $CD8^+$ T-cell depletion experiments, we further confirmed that $CD8^+$ T-cell-mediated antitumor immunity is the principal effector mechanism underlying the therapeutic efficacy of PRMT5 inhibition.

Notably, Jiang et al.[7] discovered that inhibiting PRMT5 in cervical cancer cells reduces PD-L1 levels, enhancing T-cell antitumor response. Conversely, in lung cancer, PRMT5 inhibition can activate the PD-1/PD-L1 pathway, attenuating T-cell antitumor effects[8]. In this study, we demonstrate that PRMT5 does not influence PD-L1 expression in liver cancer, indicating that the role of PRMT5 may vary across different cancers. Further results demonstrate that FGL1 is the downstream molecule of PRMT5, affecting liver cancer antitumor immunity. Wang et al.[19] demonstrated that FGL1 is a functional ligand of LAG3, and the FGL1/LAG3 pathway constitutes a promising immune checkpoint pathway independent of the PD-L1/PD-1 route. However, Maruhashi et al.[38] reported that peptide−MHC class II complexes, but not FGL1, act as the functional ligand for LAG3. Despite this, their research also indicated that FGL1 can suppress T cells. Collectively, while the functional ligand of LAG3 remains controversial, it is certain that inhibiting FGL1 can activate T cells, thereby exerting antitumor immunity. Our results demonstrate that targeting FGL1 in liver cancer cells promoted $CD8^+$ T-cell expansion and activation within the tumor microenvironment. We further demonstrated that inhibiting PRMT5 can reduce FGL1 expression, thereby enhancing $CD8^+$ T-cell antitumor immune response.

Moreover, our study elucidates that TCF12 is the transcription factor for FGL1 and acts as an intermediary in PRMT5's regulation of FGL1. As a methyltransferase, PRMT5 can boost the binding of transcription factors to DNA through arginine symmetric dimethylation, thereby promoting transcriptional activation of target genes[27,37]. Our research found that PRMT5 regulates FGL1 expression by catalyzing the symmetric dimethylation of TCF12 at the R554 residue, enhancing TCF12-mediated FGL1 transcription. The potential therapeutic value of targeting PRMT5-mediated methylation underscores a promising strategy in liver cancer management. Encouragingly, several PRMT5 inhibitors have been discovered in recent years and have demonstrated anticancer potential[29,39]. In this study, the PRMT5 inhibitor GSK591 could enhance antitumor immunity by curbing TCF12 methylation and diminishing FGL1 expression. Thus, PRMT5 inhibitors may offer a new approach to enhance antitumor immunity in liver cancer.

The inhibitory immune checkpoints, such as PD-1/PD-L1 and FGL1/LAG3, are well-known for inhibiting T cells and assisting tumor cells to evade immune destruction[19,40]. Blocking these checkpoints can release the immune brake, thus enhancing T-cell antitumor effects. However, liver cancer is an immunosuppressive malignancy with a poor response rate to anti-PD-L1 treatment[13]. Given that FGL1 independently regulates T-cell activity from PD-L1, targeting both checkpoints theoretically should yield a synergistic antitumor response. Lin et al.[22] uncovered that aspirin

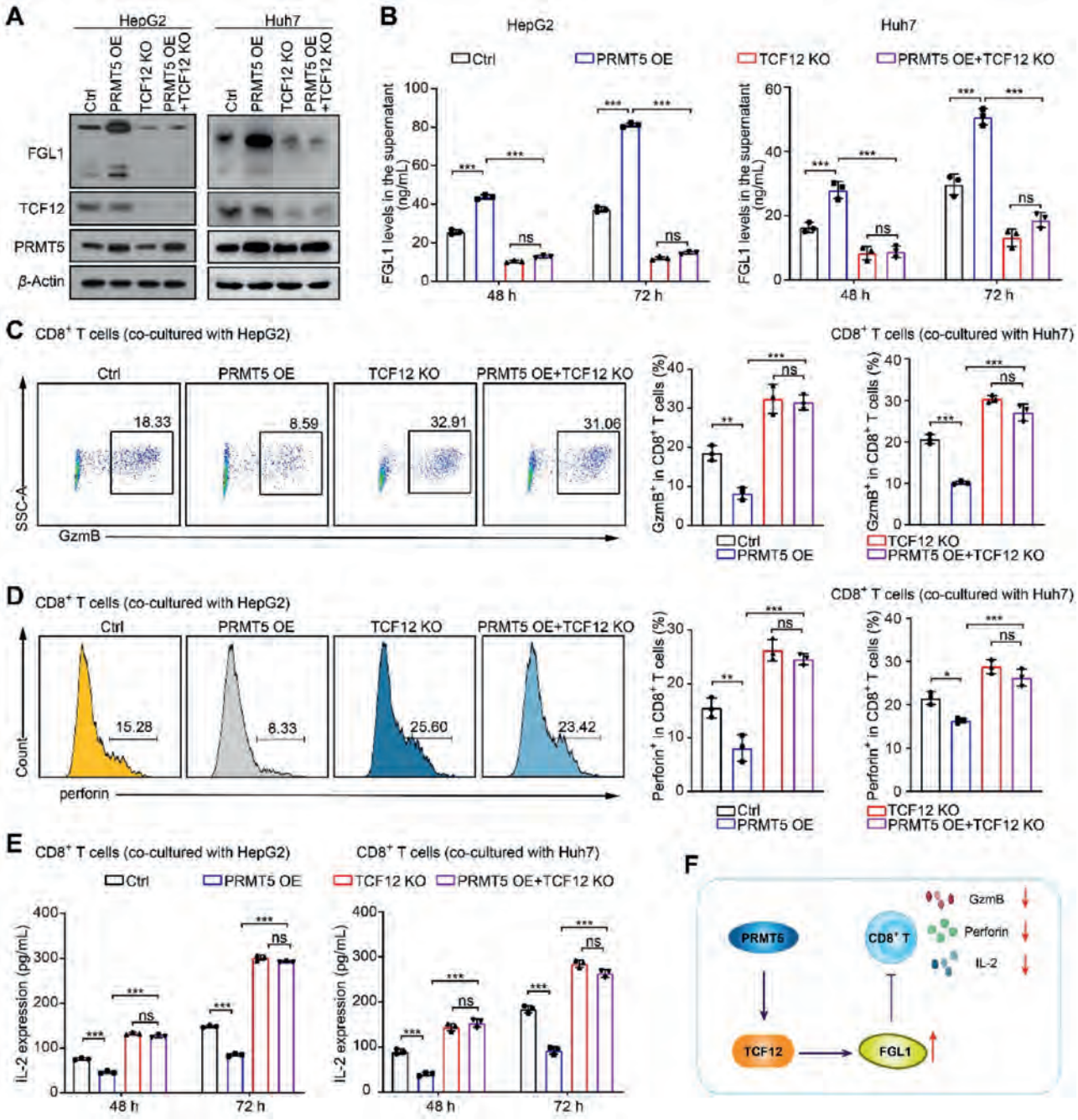

Figure 6 PRMT5 suppresses $CD8^+$ T-cell activity *via* TCF12/FGL1 axis *in vitro*. (A, B) HepG2 and Huh7 cells were treated with PRMT5 OE, TCF12 KO or simultaneously. (A) Protein levels of FGL1, TCF12 and PRMT5 in each group were assessed by Western blot analysis. (B) Secreted FGL1 protein levels in the supernatant were assessed after 48 and 72 h using ELISA. (C−E) $CD8^+$ T cells were co-cultured with indicated HepG2 or Huh7 cells. Flow cytometry quantification of $GzmB^+$ (C) and $Perforin^+$ (D) cell proportions within $CD8^+$ T cells. (E) IL-2 expression levels in the co-culture supernatant were measured after 48 and 72 h using ELISA. (F) The schematic diagram illustrating the influence of the PRMT5/TCF12/FGL1 axis on $CD8^+$ T-cell activity. $^*P < 0.05$, $^{**}P < 0.01$, $^{***}P < 0.001$; ns: no significance. KO: knockout, OE: overexpression, GzmB: granzyme B, IL-2: interleukin 2.

promotes the degradation of FGL1 and sensitizes hepatocellular carcinoma to anti-PD-L1 therapy. Gong et al.[41] demonstrated that the application of nanoparticles encapsulating si-FGL1 in breast cancer effectively enhances T-cell-mediated antitumor immunity and produces synergistic effects with anti-PD-L1 treatment. In liver metastatic tumor models, benzethonium chloride activates antitumor immunity by inhibiting FGL1 secretion and synergizes with anti-PD-1 treatment[42]. In this study, we demonstrated that the PRMT5 inhibitor GSK591 could reduce FGL1 expression in liver cancer cells. Combining GSK591 with anti-PD-L1 therapy enhances the antitumor immune response, presenting a more effective tumor suppression effect.

In conclusion, our research demonstrates that tumor-intrinsic PRMT5 upregulates FGL1 by methylating TCF12, thereby

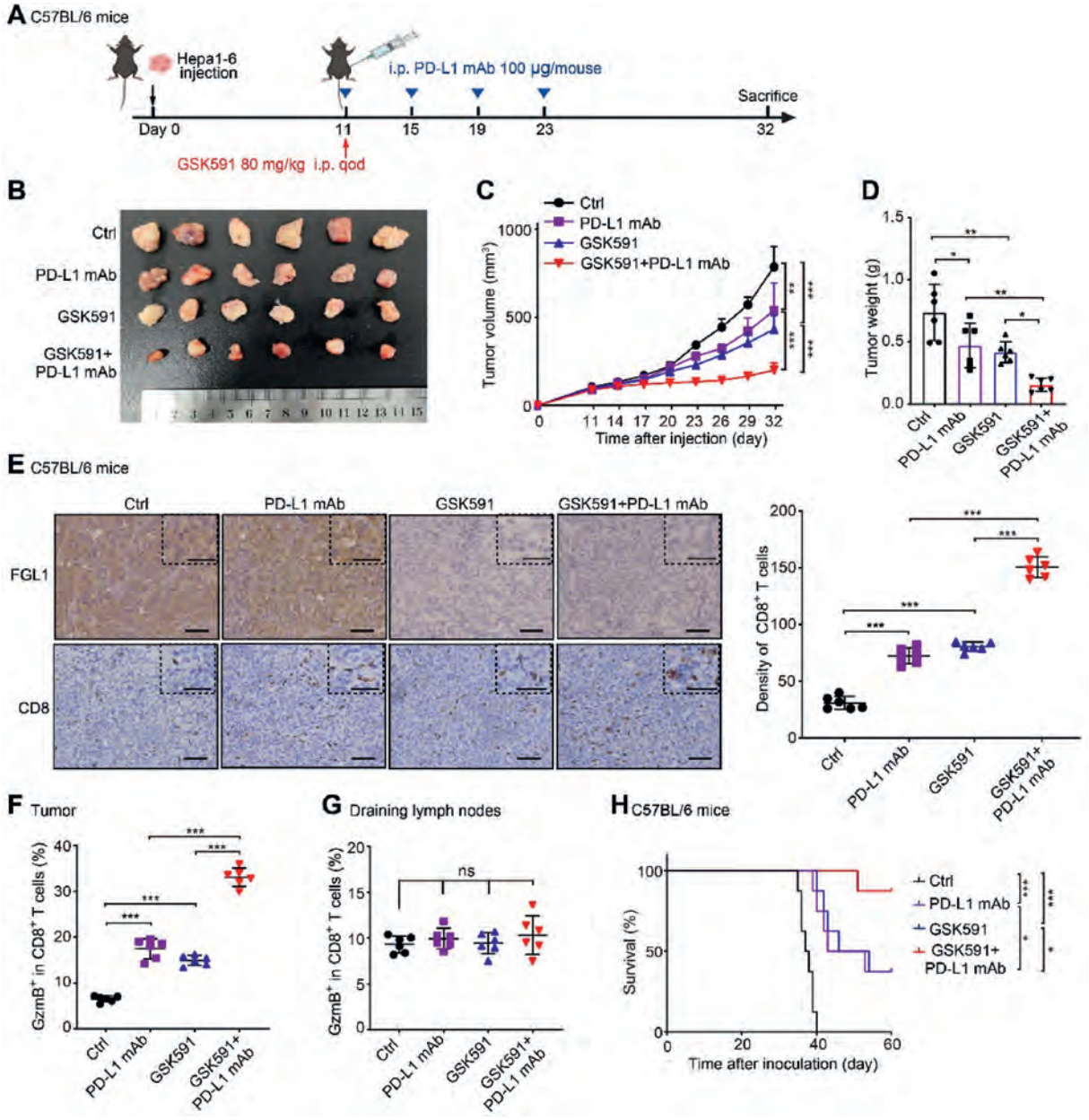

Figure 7 PRMT5 inhibitor boosts PD-L1 mAb sensitivity in liver cancer immunotherapy. (A) Schematic representation of the animal experimental design. (B−D) Tumor appearance (B), volume (C), and weights (D) in Ctrl, PD-L1 mAb, GSK591, and GSK591 + PD-L1 mAb groups ($n = 6$). (E) Representative IHC images of FGL1 and $CD8^+$ T cells (left), and quantification of $CD8^+$ T cells (right) ($n = 6$). Scale bar, 50 μm. (F, G) Flow cytometry quantifying frequency of $GzmB^+$ cells in $CD8^+$ T cells in tumor tissues (F) and draining lymph nodes (G) ($n = 6$). (H) Survival analysis across 4 groups ($n = 8$). $^*P < 0.05$, $^{**}P < 0.01$, $^{***}P < 0.001$; ns: no significance. mAb: monoclonal antibody, GzmB: granzyme B.

inhibiting $CD8^+$ T-cell-mediated antitumor immunity. The combination of the PRMT5 inhibitor GSK591 with anti-PD-L1 therapy produces more effective antitumor effects, offering a promising strategy for the immunotherapy of liver cancer (Supporting Information Fig. S6).

Acknowledgments

This work was supported by the National Natural Science Foundation of China (Nos. 82372818 to Xiaodong Zhang, 82103066 to Guang Yang, 82302887 to Hongfeng Yuan, 82303210 to Yufei Wang). The China Postdoctoral Science Foundation (No. 2022M712389 to Hongfeng Yuan; No. 2023M732624 to Yufei Wang; No. 2023M742621 to Lina Zhao), Tianjin Key Medical Discipline (Specialty) Construction Project (TJYXZDXK-009A to W. Lu, China), "14th Five-Year Plan" Tumor Prevention and Treatment Research Project of Tianjin Medical University Cancer Institute and Hospital (No. YZ-03, China).

Author contributions

Jiao Sun: Writing − original draft, Visualization, Validation, Software, Project administration, Methodology, Investigation, Formal analysis, Data curation, Conceptualization. Hongfeng

Yuan: Visualization, Funding acquisition, Data curation. Linlin Sun: Software, Investigation, Data curation. Lina Zhao: Validation, Supervision. Yufei Wang: Software, Project administration. Chunyu Hou: Validation, Software. Huihui Zhang: Validation, Formal analysis. Pan Lv: Supervision, Methodology. Guang Yang: Writing − review & editing, Funding acquisition, Conceptualization. Ningning Zhang: Project administration, Conceptualization. Wei Lu: Writing − review & editing, Project administration, Funding acquisition, Conceptualization. Xiaodong Zhang: Writing − review & editing, Project administration, Funding acquisition, Conceptualization.

Conflicts of interest

The authors have declared that no competing interest exists.

Appendix A. Supporting information

Supporting information to this article can be found online at https://doi.org/10.1016/j.apsb.2024.10.016.

References

1. Singal AG, Kanwal F, Llovet JM. Global trends in hepatocellular carcinoma epidemiology: implications for screening, prevention and therapy. *Nat Rev Clin Oncol* 2023;**20**:864−84.
2. Park JW, Chen M, Colombo M, Roberts LR, Schwartz M, Chen PJ, et al. Global patterns of hepatocellular carcinoma management from diagnosis to death: the BRIDGE Study. *Liver Int* 2015;**35**:2155−66.
3. Chakraborty E, Sarkar D. Emerging therapies for hepatocellular carcinoma (HCC). *Cancers (Basel)* 2022;**14**:2798.
4. Sia D, Jiao Y, Martinez-Quetglas I, Kuchuk O, Villacorta-Martin C, Castro de Moura M, et al. Identification of an immune-specific class of hepatocellular carcinoma, based on molecular features. *Gastroenterology* 2017;**153**:812−26.
5. Boisvert FM, Côté J, Boulanger MC, Richard S. A proteomic analysis of arginine−methylated protein complexes. *Mol Cell Proteomics* 2003;**2**:1319−30.
6. Lacroix M, El Messaoudi S, Rodier G, Le Cam A, Sardet C, Fabbrizio E. The histone-binding protein COPR5 is required for nuclear functions of the protein arginine methyltransferase PRMT5. *EMBO Rep* 2008;**9**:452−8.
7. Jiang Y, Yuan Y, Chen M, Li S, Bai J, Zhang Y, et al. PRMT5 disruption drives antitumor immunity in cervical cancer by reprogramming T cell-mediated response and regulating PD-L1 expression. *Theranostics* 2021;**11**:9162−76.
8. Hu R, Zhou B, Chen Z, Chen S, Chen N, Shen L, et al. PRMT5 inhibition promotes PD-L1 expression and immuno-resistance in lung cancer. *Front Immunol* 2021;**12**:722188.
9. Li Z, Zhang J, Liu X, Li S, Wang Q, Di C, et al. The LINC01138 drives malignancies *via* activating arginine methyltransferase 5 in hepatocellular carcinoma. *Nat Commun* 2018;**9**:1572.
10. Zheng BN, Ding CH, Chen SJ, Zhu K, Shao J, Feng J, et al. Targeting PRMT5 activity inhibits the malignancy of hepatocellular carcinoma by promoting the transcription of HNF4α. *Theranostics* 2019;**9**: 2606−17.
11. Sharma P, Hu-Lieskovan S, Wargo JA, Ribas A. Primary, adaptive, and acquired resistance to cancer immunotherapy. *Cell* 2017;**168**:707−23.
12. Yi M, Zheng X, Niu M, Zhu S, Ge H, Wu K. Combination strategies with PD-1/PD-L1 blockade: current advances and future directions. *Mol Cancer* 2022;**21**:28.
13. Llovet JM, Castet F, Heikenwalder M, Maini MK, Mazzaferro V, Pinato DJ, et al. Immunotherapies for hepatocellular carcinoma. *Nat Rev Clin Oncol* 2022;**19**:151−72.
14. Anderson AC, Joller N, Kuchroo VK. Lag-3, Tim-3, and TIGIT: co-inhibitory receptors with specialized functions in immune regulation. *Immunity* 2016;**44**:989−1004.
15. Kraehenbuehl L, Weng CH, Eghbali S, Wolchok JD, Merghoub T. Enhancing immunotherapy in cancer by targeting emerging immunomodulatory pathways. *Nat Rev Clin Oncol* 2022;**19**:37−50.
16. Ruffo E, Wu RC, Bruno TC, Workman CJ, Vignali DAA. Lymphocyte-activation gene 3 (LAG3): the next immune checkpoint receptor. *Semin Immunol* 2019;**42**:101305.
17. Workman CJ, Vignali DA. Negative regulation of T cell homeostasis by lymphocyte activation gene-3 (CD223). *J Immunol* 2005;**174**:688−95.
18. Chihara N, Madi A, Kondo T, Zhang H, Acharya N, Singer M, et al. Induction and transcriptional regulation of the co-inhibitory gene module in T cells. *Nature* 2018;**558**:454−9.
19. Wang J, Sanmamed MF, Datar I, Su TT, Ji L, Sun J, et al. Fibrinogen-like protein 1 is a major immune inhibitory ligand of LAG-3. *Cell* 2019;**176**:334−47.e12.
20. Yang C, Qian Q, Zhao Y, Huang B, Chen R, Gong Q, et al. Fibrinogen-like protein 1 promotes liver-resident memory T-cell exhaustion in hepatocellular carcinoma. *Front Immunol* 2023;**14**:1112672.
21. Yan Q, Lin HM, Zhu K, Cao Y, Xu XL, Zhou ZY, et al. Immune checkpoint FGL1 expression of circulating tumor cells is associated with poor survival in curatively resected hepatocellular carcinoma. *Front Oncol* 2022;**12**:810269.
22. Lin M, He J, Zhang X, Sun X, Dong W, Zhang R, et al. Targeting fibrinogen-like protein 1 enhances immunotherapy in hepatocellular carcinoma. *J Clin Invest* 2023;**133**:e164528.
23. Yuan HF, Zhao M, Zhao LN, Yun HL, Yang G, Geng Y, et al. PRMT5 confers lipid metabolism reprogramming, tumour growth and metastasis depending on the SIRT7-mediated desuccinylation of PRMT5 K387 in tumours. *Acta Pharmacol Sin* 2022;**43**:2373−85.
24. Yuan H, Zhao L, Yuan Y, Yun H, Zheng W, Geng Y, et al. HBx represses WDR77 to enhance HBV replication by DDB1-mediated WDR77 degradation in the liver. *Theranostics* 2021;**11**:8362−78.
25. Fu Y, Alashi AM, Young JF, Therkildsen M, Aluko RE. Enzyme inhibition kinetics and molecular interactions of patatin peptides with angiotensin I-converting enzyme and renin. *Int J Biol Macromol* 2017; **101**:207−13.
26. Tu M, Liu H, Zhang R, Chen H, Mao F, Cheng S, et al. Analysis and evaluation of the inhibitory mechanism of a novel angiotensin-I-converting enzyme inhibitory peptide derived from casein hydrolysate. *J Agric Food Chem* 2018;**66**:4139−44.
27. Wei H, Wang B, Miyagi M, She Y, Gopalan B, Huang DB, et al. PRMT5 dimethylates R30 of the p65 subunit to activate NF-κB. *Proc Natl Acad Sci U S A* 2013;**110**:13516−21.
28. Massari ME, Murre C. Helix−loop−helix proteins: regulators of transcription in eucaryotic organisms. *Mol Cell Biol* 2000;**20**:429−40.
29. Richters A. Targeting protein arginine methyltransferase 5 in disease. *Future Med Chem* 2017;**9**:2081−98.
30. Mersaoui SY, Yu Z, Coulombe Y, Karam M, Busatto FF, Masson JY, et al. Arginine methylation of the DDX5 helicase RGG/RG motif by PRMT5 regulates resolution of RNA:DNA hybrids. *Embo j* 2019;**38**: e100986.
31. Thandapani P, O'Connor TR, Bailey TL, Richard S. Defining the RGG/RG motif. *Mol Cell* 2013;**50**:613−23.
32. An W, Kim J, Roeder RG. Ordered cooperative functions of PRMT1, p300, and CARM1 in transcriptional activation by p53. *Cell* 2004;**117**: 735−48.
33. Rezai-Zadeh N, Zhang X, Namour F, Fejer G, Wen YD, Yao YL, et al. Targeted recruitment of a histone H4-specific methyltransferase by the transcription factor YY1. *Genes Dev* 2003;**17**:1019−29.
34. Covic M, Hassa PO, Saccani S, Buerki C, Meier NI, Lombardi C, et al. Arginine methyltransferase CARM1 is a promoter-specific regulator of NF-κB-dependent gene expression. *EMBO J* 2005;**24**:85−96.
35. Jiang H, Zhu Y, Zhou Z, Xu J, Jin S, Xu K, et al. PRMT5 promotes cell proliferation by inhibiting BTG2 expression *via* the ERK signaling pathway in hepatocellular carcinoma. *Cancer Med* 2018;**7**: 869−82.

36. Zhu K, Peng Y, Hu J, Zhan H, Yang L, Gao Q, et al. Metadherin−PRMT5 complex enhances the metastasis of hepatocellular carcinoma through the WNT−β-catenin signaling pathway. *Carcinogenesis* 2020;**41**:130−8.
37. Liu L, Zhao X, Zhao L, Li J, Yang H, Zhu Z, et al. Arginine methylation of SREBP1a *via* PRMT5 promotes *de novo* lipogenesis and tumor growth. *Cancer Res* 2016;**76**:1260−72.
38. Maruhashi T, Sugiura D, Okazaki IM, Shimizu K, Maeda TK, Ikubo J, et al. Binding of LAG-3 to stable peptide-MHC class II limits T cell function and suppresses autoimmunity and anti-cancer immunity. *Immunity* 2022;**55**:912−24.e8.
39. Luo Y, Gao Y, Liu W, Yang Y, Jiang J, Wang Y, et al. Myelocytomatosis-protein arginine *N*-methyltransferase 5 axis defines the tumorigenesis and immune response in hepatocellular carcinoma. *Hepatology* 2021;**74**:1932−51.
40. Jiang X, Wang J, Deng X, Xiong F, Ge J, Xiang B, et al. Role of the tumor microenvironment in PD-L1/PD-1-mediated tumor immune escape. *Mol Cancer* 2019;**18**:10.
41. Gong C, Yu X, Zhang W, Han L, Wang R, Wang Y, et al. Regulating the immunosuppressive tumor microenvironment to enhance breast cancer immunotherapy using pH-responsive hybrid membrane-coated nanoparticles. *J Nanobiotechnology* 2021;**19**:58.
42. Li JJ, Wang JH, Tian T, Liu J, Zheng YQ, Mo HY, et al. The liver microenvironment orchestrates FGL1-mediated immune escape and progression of metastatic colorectal cancer. *Nat Commun* 2023;**14**:6690.